Astron. Astrophys. 344, 289–294 (1999)

ASTRONOMY AND ASTROPHYSICS

A comparison of the X-ray line and continuum morphology of Cassiopeia A

Jacco Vink[1], M. Concetta Maccarone[2], Jelle S. Kaastra[1], Teresa Mineo[2], Johan A.M. Bleeker[1], Andrea Preite-Martinez[3], and Hans Bloemen[1]

[1] SRON Laboratory for Space Research, Sorbonnelaan 2, 3584 CA Utrecht, The Netherlands
[2] Istituto di Fisica Cosmica ed Applicazioni all'Informatica, CNR, Via U. La Malfa 153, I-90146 Palermo, Italy
[3] Istituto di Astrofisica Spaziale, Area di Ricerca di Tor Vergata, Via del Fosso del Cavaliere 133, Roma, Italy

Received 22 October 1998 / Accepted 22 January 1999

Abstract. We present deconvolved narrow band images of Cas A as observed by the MECS instrument on the BeppoSAX X-ray satellite. The images show that Cas A has different morphologies in the continuum and line bands. This difference points towards a synchrotron origin for part of the X-ray continuum of Cas A. Going to the hardest continuum band we find that the emission is coming predominantly from the Western region, making this the most likely location for the hard X-ray tail seen with instruments on CGRO (OSSE), BeppoSAX (PDS) and RXTE (HEXTE).

Key words: X-rays: ISM – ISM: supernova remnants – ISM: cosmic rays – ISM: individual objects: Cas A

1. Introduction

The X-ray emission from supernova remnants has generally been understood to be thermal emission (i.e. bremsstrahlung and line emission) for the so called shell type supernova remnants, such as Tycho, Kepler and Cassiopeia A (Cas A), and synchrotron emission for the plerions such as the Crab nebula. In the latter case the synchrotron emission is caused by cosmic ray electrons accelerated in the magnetosphere surrounding the neutron star. The ideas on shell type remnants have, however, changed dramatically with the publication of the analysis of ASCA data of the remnant of SN1006 by Koyama et al. (1995). They proposed that the featureless X-ray spectra of the rims of the remnant were the result of synchrotron emission (earlier anticipated by Reynolds & Chevalier 1981). SN1006 is a shell type remnant and does not contain, as far as we know, a pulsar, hence the synchrotron emission should arise from cosmic ray electrons accelerated in the blast wave of the supernova remnant. This view is supported by the recent discovery of TeV gamma rays coming from the Northeastern rim of SN1006 (Tanimori et al. 1998).

Of course, if there is X-ray synchrotron radiation coming from SN1006, then it is very likely that other (young) shell type remnants also produce synchrotron radiation at some level. Although, it is worth pointing out that SN 1006 was probably a type Ia supernova, whereas Cas A is very likely the remnant of a core collapse supernova (Type Ib or II). Recently, a hard X-ray tail was discovered in the spectrum of Cas A, the youngest known galactic supernova remnant (The et al. 1996, Favata et al. 1997, Allen et al. 1997). This tail can be attributed to synchrotron radiation, but it could also arise from bremsstrahlung caused by a non-Maxwellian tail to the thermal electron distribution. Note that, like SN1006, Cas A does not seem to contain a pulsar. In the case of Cas A there is no doubt that a substantial part of the emission is thermal in nature, since the remnant displays strong line emission. So, whatever the nature of the hard tail, at lower photon energies this component is intermingled with thermal components.

From a theoretical point of view both synchrotron emission (Reynolds 1997) and non-thermal bremsstrahlung can exist (Asvarov et al. 1990). For instance, the cosmic ray electrons responsible for the radio emission of Cas A find their origin in thermal electrons accelerated at the shock. This means that at all energies intermediate between the thermal electron distribution and the relativistic electrons responsible for the radio emission, a population of electrons should exist. The Coulomb equilibration process is slow, so if at some moment the initial electron distribution is non-thermal, the relaxation towards a Maxwellian distribution is likely to evolve slowly (Laming 1998), because the relaxation time scales with electron energy (E) as $E^{-3/2}$. To give an example applicable to Cas A ($n_{\rm e} \sim 10$ cm^{-3}): at 1 keV the relaxation time is ~ 1 yr, at 10 keV it is ~ 30 yr, and at 50 keV its is of the order of the age of the remnant. Therefore, from say 20 keV to 1 GeV the electron distribution should be a continuously decreasing function and non-thermal bremsstrahlung should exist, but may be less pronounced than the synchrotron emission.

So, what can we say at present about the relative contributions of a synchrotron component and a non-thermal bremsstrahlung component to the hard X-ray tail? Ultimately this will be resolved by observing X-ray polarization, which is not feasible presently. Here we attempt to bring the discussion somewhat further by investigating the spatial distribution of the X-ray

Send offprint requests to: J. Vink (J.Vink@sron.nl)

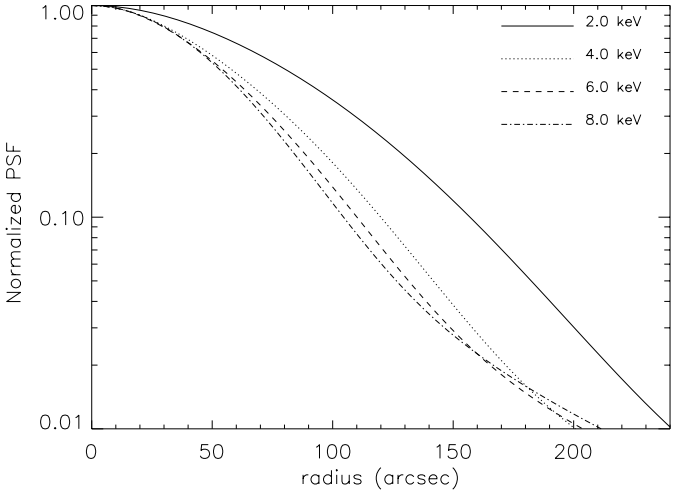

Fig. 1. The MECS3 point spread function at four energies: 2 keV, 4 keV, 6 keV and 8 keV.

emission up to 10.5 keV. We do this by presenting deconvolved images in narrow bands obtained by the MECS instrument on board BeppoSAX.

Before discussing our analysis, a short characterization of Cas A. The remnant is at a distance of $3.4^{+0.3}_{-0.1}$ kpc (Reed et al. 1995) and is between 340 and 318 years old. The younger age is based on the possible explosion date of 1680, when Flamsteed observed an unidentified 6th magnitude star near the current position of Cas A (Ashworth 1980). The older age is based on the expansion analysis of optical filaments (van den Bergh & Kamper 1983). The current wisdom is that the progenitor was probably an early type Wolf-Rayet star (Fesen et al. 1987) with an initial mass of about $30M_{\odot}$ (Garciá-Segura et al. 1996) and a final mass less than $10M_{\odot}$ (Vink et al. 1996). Recent expansion studies of high resolution X-ray images indicate that the current overall expansion velocity is ~ 3200 km s^{-1} for the bright shell and ~ 5200 km s^{-1} for the fainter emission associated with the blast wave (Vink et al. 1998, Koralesky et al. 1998). This is considerably greater than the expansion of the bright radio ring which is about 2000 km s^{-1} (Anderson & Rudnick 1995).

2. Observations and analysis

2.1. The data

The BeppoSAX satellite (Boella et al. 1997a) contains four X-ray detectors: the LECS (0.1–10 keV) and MECS (1.5–12 keV), composed of three units, the HPGSPC (4–120 keV) and the PDS (13–300 keV). The overall spectrum of Cas A as observed by BeppoSAX is shown in the paper by Favata et al. (1997). Only the LECS and MECS have imaging capabilities. Here we have opted for only using the MECS (Boella et al. 1997b) instrument, since the supporting structure of the LECS blocks part of the field of view, whereas the MECS has an unobstructed view of Cas A, which simplifies the image analysis considerably. Furthermore, the MECS has a higher sensitivity above 5 keV than the LECS. BeppoSAX observed Cas A five times; four observations during the performance verification phase in August and September 1996 and one observation on November 26, 1997. The total observation time is different for each set of instruments, but data presented here comprise 161 ks of MECS observation time. The data analyzed here are based on the MECS2 and MECS3 units (labeled together as MECS23) for uniformity: the MECS1 was no longer functioning at the time of the last observation. Comparing the various data sets we found that there were rather large inaccuracies in the aspect solutions. This was most distinct for the last observation ($\sim 1.4'$) made after a gyroscope failure, which may have caused the relatively large error in the aspect solution. Using a correlation analysis similar to that employed by Vink et al. (1998), we shifted the observations in order to match in position.

2.2. Lucy-Richardson deconvolution

The MECS point spread function (PSF) consists of two components, representing the gaussian shaped intrinsic resolution of the MECS instrument and the scattering component originating from the mirrors. These components can be identified in the following parameterization of the PSF as a function of radius, r, (Boella et al. 1997b):

$$f(r) = C\{\alpha \exp(-\frac{1}{2}\frac{r^2}{\sigma^2}) + (1.0 + \frac{r^2}{R^2})^{-\beta}\}; \quad (1)$$

note that the parameters σ, R, α and β are energy dependent (S. Molendi, private communication). C is a normalization constant, so that the integration over the total plane equals 1. Fig. 1 shows the PSF of the MECS3 for four different energies. As can be seen the PSF changes with energy, especially the change from 2 to 4 keV is dramatic. Above 4 keV the PSF does not change much anymore. At higher energies the resolution of the MECS increases, but the mirror scattering becomes worse. Fortunately, the photon statistics at 2 keV are far superior to those at 8 keV, so we can compensate for the degraded resolution at 2 keV by performing more iterations of the deconvolution algorithm.

We used the analytical representation of the PSF to deconvolve the narrow band MECS images with the Lucy-Richardson deconvolution algorithm (Lucy 1974, Richardson 1972). One problem associated with this algorithm is the number of iterations that should be used. Too many iterations may cause spurious results, too few iterations do not bring out the full potential of the image. We solved this by statistically comparing the convolved model image with the raw image at each iterative step; when the model improvements were less than 1σ we halted the deconvolution process. The consistency of our results was verified by comparing the deconvolved images of individual datasets with those of the total dataset and, as discussed below, with the results from other X-ray telescopes. We point out that some of the features presented below were already recognizable in the raw images (Maccarone et al. 1998).

2.3. Comparison with previous measurements

We present here the first analysis of the morphology of Cas A for photon energies in excess of 6 keV. A similar analysis was

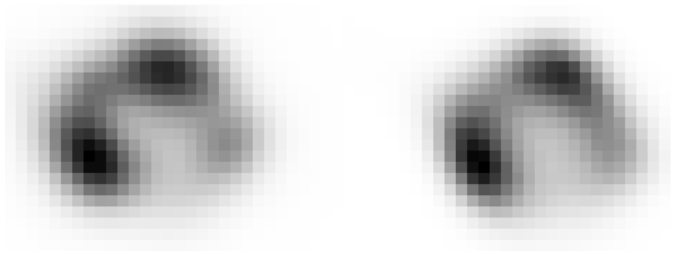

Fig. 2. A comparison of the MECS23 image in the silicon band (on the *right*) with the ROSAT PSPC image from ~ 1.5 keV to ~ 2.3 keV convolved with a gaussian with $\sigma = 24''$.

Table 1. The energy ranges and number of iterations for the Lucy-Richardson deconvolution used for the images. Images dominated by line emission are labeled with the element producing the line emission. In all cases the emission consists of blends of lines of H-like and He-like ions.

characterization	energy range keV	# iterations
Si	1.6–2.4	440
S	2.4–2.9	244
Ar	2.9–3.3	158
continuum	4.0–6.0	117
Fe K	6.1–7.1	114
continuum	7.3–9.0	64
continuum	9.0–10.6	43

done with ASCA SIS0 data for energies below 6 keV (Holt et al. 1994). The advantage of the MECS instrument over ASCA SIS is that it is more sensitive above 6 keV and also the PSF of the MECS is simpler. The core of the MECS PSF is, however, broader than for the ASCA SIS, so that the deconvolved MECS images in the range 1.8 keV to 6 keV do not show as much detail as the deconvolved SIS images. Apart from the lack of detail, the MECS images below 6 keV are in agreement with the images presented by Holt et al. (1994).

A comparison of the ROSAT PSPC image with the deconvolved silicon image provides another check on the validity of our results. As can be seen in Fig. 2 the images compare well.

3. Results

The deconvolved narrow band images are displayed in Fig. 3; the energy ranges and the number of Lucy-Richardson iterations are listed in Table 1. In Fig. 3 we have ordered the images such that images dominated by line emission are on the left side and continuum images are on the right. For comparison we included an archival VLA image showing synchrotron emission at a wavelength of 21.7 cm. This image has been smoothed to roughly the same resolution as the deconvolved MECS images.

It is immediately clear that the spatial distribution of the continuum emission is different from the line emission, whereas the images relating to the line emission do not differ much from one another. The silicon image is not so bright in the West, but this is due to the fact that this part of the remnant is more absorbed

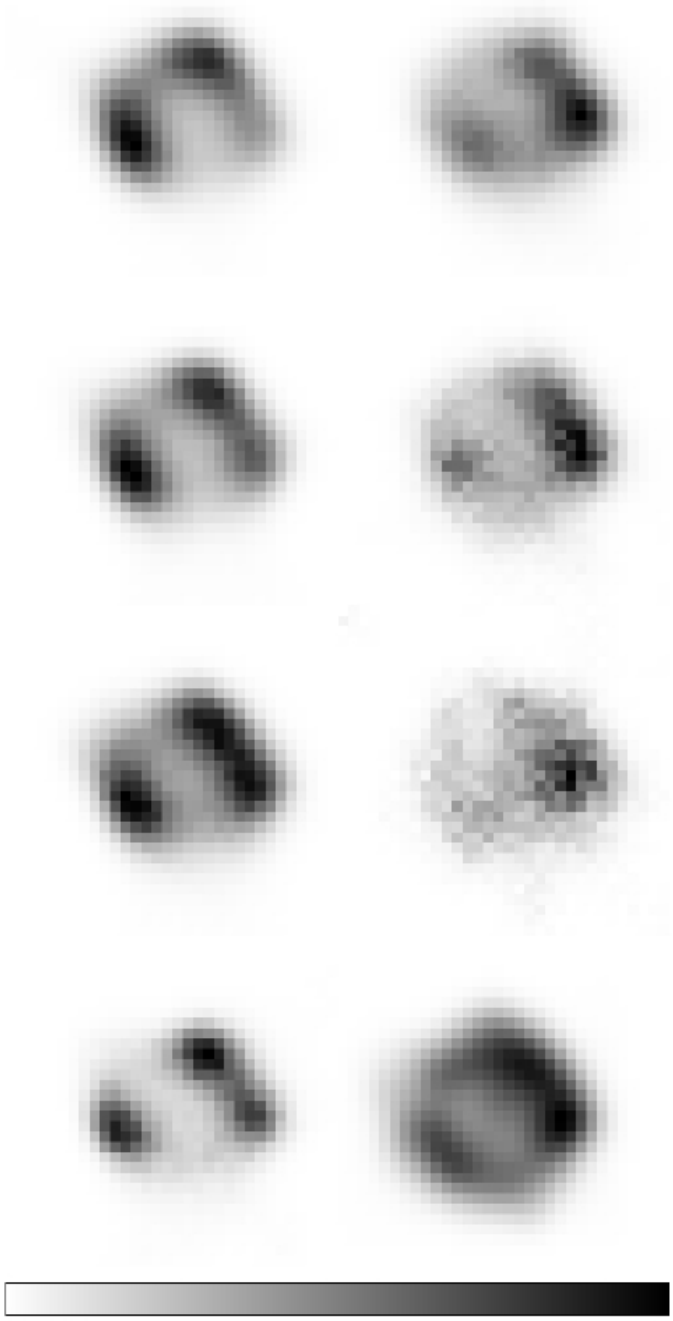

Fig. 3. The deconvolved MECS23 images. On the *left:* image dominated by line emission from Si, S, Ar and Fe. On the *right:* continuum emission in the energy ranges 4–6 keV, 7.3–9 keV, 9–10.6 keV and a VLA image convolved with a Gaussian with $\sigma = 24''$. Note that the line images are not corrected for the continuum distribution, which will affect the Ar and Fe K image most.

by the interstellar medium than the rest of Cas A (Keohane et al. 1998). There is also a hint in the Fe K band image that the iron line emission in the Southeast peaks further out from the center of the remnant than the line emission of Si, S and Ar. The displacement is about $20''$, as can be seen in Fig. 4. This may indicate that the iron emission in that area is predominantly coming from the shocked circumstellar medium rather than from the

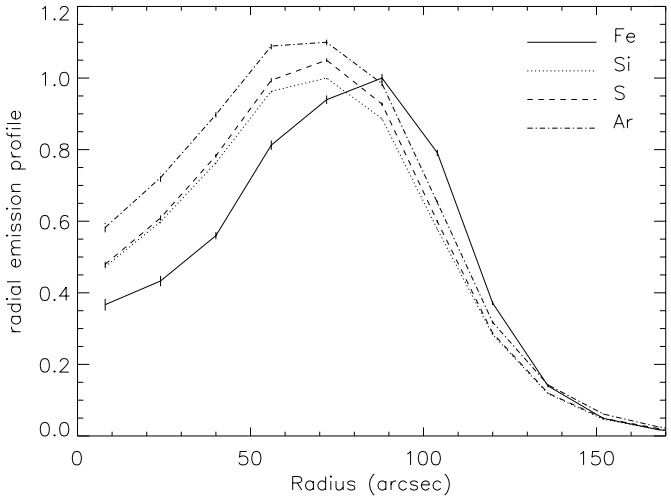

Fig. 4. The radial profiles for the Southeastern region (45° to 170° from the North). The iron emission peaks about 20″ further from the center than the emission from Si, S and Ar.

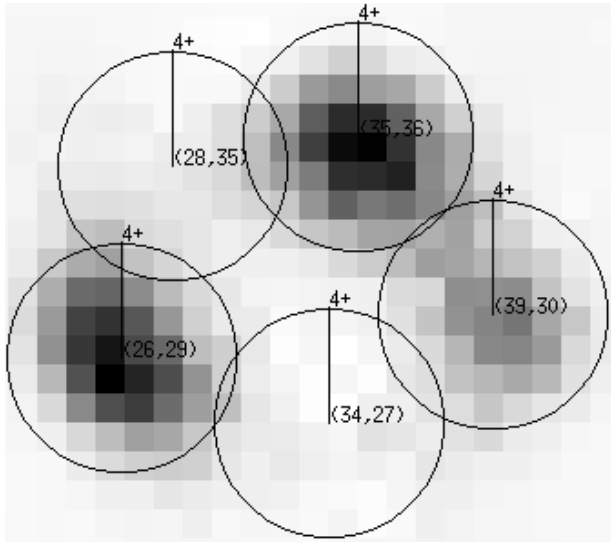

Fig. 5. This image (the deconvolved, continuum subtracted iron K image) shows the regions used for producing Fig. 6. North is up.

shocked ejecta. The lack of variation from one line image to the other indicates that dust depletion cannot play a major role in explaining the line radiation morphology, since silicon and iron can be easily dust depleted, whereas sulphur and argon cannot.

The continuum emission does vary strongly from one energy band to another, but the continuum images differ from the line emission images in that they all peak in the Western region of the remnant, a property they share with the VLA image.

In order to make more quantitative statements we concentrate on the emission above 4 keV. Each image was corrected for the bandwidth and instrument effective area, so that the pixel values correspond to the approximate flux density per pixel (i.e. photons $\mathrm{keV}^{-1}\mathrm{m}^{-2}\,\mathrm{s}^{-1}\mathrm{pixel}^{-1}$, one pixel being 16″ in size). With these images rough spectra at various regions were made (see Fig. 5 for the regions). This is shown in Fig. 6 and useful

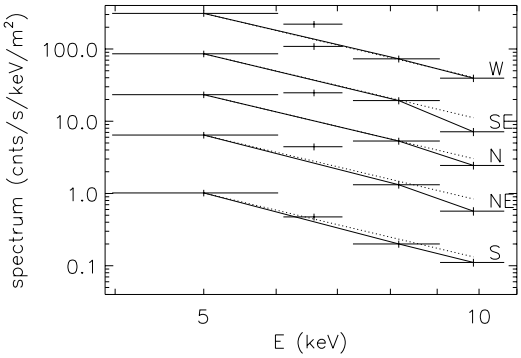

Fig. 6. Spectra in the energy range 4.0–10.6 keV reconstructed from the deconvolved images. The different spectra are for circular regions with radii of 64″. The vertical error bars represent 5% errors, the horizontal bar shows the energy ranges. The solid lines indicate the assumed continuum emission. The dotted lines show spectra with a power law index of 3. The spectra have been rescaled for reasons of clarity.

Table 2. The results of the analysis of the continuum and Fe K band images (cf. Fig. 6). The errors include 5% systematic errors for the flux measurements. Γ is the power law index. The index @ 6.6 keV is based on the 4–6 keV and 7.3–9 keV images and the index @ 9.0 keV is based on the 7.3–9 keV and 9–10.6 keV images.

region	EW Fe Kα keV	Γ @ 6.6 keV	Γ @ 9.0 keV
Northeast	0.69 ± 0.12	3.2 ± 0.2	4.5 ± 0.6
North	1.45 ± 0.18	3.0 ± 0.2	4.2 ± 0.5
West	0.61 ± 0.12	3.0 ± 0.2	3.3 ± 0.5
South	0.17 ± 0.09	3.3 ± 0.2	3.2 ± 0.5
Southeast	1.94 ± 0.22	3.0 ± 0.2	5.4 ± 0.5

parameters related to the spectra are listed in Table 2. The statistical errors of the flux measurements are small, so the systematic errors, which are of the order of 5%, dominate. We corrected the iron image for the continuum contribution. Dividing this image by the estimated continuum emission at 6.6 keV we ended up with an image approximating the equivalent width of the iron K-shell emission (Fig. 7). The peak equivalent width in Fig. 7 of 4.7 keV is rather high, but the average equivalent width per region, as determined from the images, agrees with the value in Table 2 and spectral analysis results.

The continuum in the iron band image was estimated by interpolating the 4–6 keV and 7.3–9.0 keV image to 6.6 keV assuming a photon index of 3.0 and averaging those two continuum images. The results, shown in Fig. 6, Fig. 7 and Table 2, confirm that the line emission peaks in the North and Southeast, whereas the continuum peaks in the West. The Western regions becomes relatively brighter at higher energies.

If line emission is an indication for a thermal origin of the emission, is its prominent absence a signature for synchrotron emission? It seems at least the most natural explanation, since other explanations involving steep abundance gradients or anomalous electron distributions are more far fetched. This argument is supported by the observation that all the line images

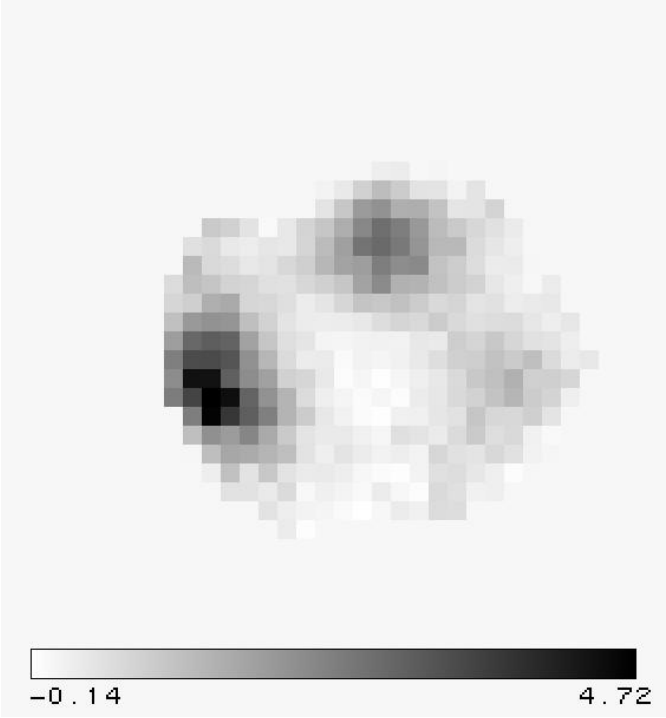

Fig. 7. This image represents the iron K-shell emission equivalent width (in keV). Negative values, which are unphysical, have been removed at the edge of the remnant. Pixels are 16″ in size.

have rather similar morphologies, so if there are abundance gradients they should be roughly equal for all elements. Non-thermal bremsstrahlung does not explain the difference between the continuum morphology and the line morphology, because the electrons involved in this process should also cause line emission. The line emission does indicate, however, that there is also a contribution of bremsstrahlung to the continuum. The bending of the spectra in some regions shown in Fig. 6 (e.g. the Southeastern and Northeastern regions) indicates that the continua in those regions are probably dominated by thermal-bremsstrahlung, whereas the Western and Southern regions are likely to be dominated by synchrotron emission. The trends visible in the continuum images make it very likely that the hard X-ray tail above 20 keV (The et al. 1996, Favata et al. 1997, Allen et al. 1997) is coming predominantly from the West of Cas A.

Models for the X-ray synchrotron emission of shell type supernova remnants (e.g. Reynolds 1997) predict that the synchrotron spectrum extrapolated from the radio emission should cut off with a term shallower than $\exp(-(\frac{E}{E_c})^{\frac{1}{2}})$, with E the photon energy and E_c the cut off energy. From this we can derive that the photon index, Γ, of the X-ray spectrum is given by:

$$\Gamma = \alpha_R + \frac{1}{2}(\frac{E}{E_c})^{\frac{1}{2}} + 1, \quad (2)$$

with α_R the radio spectral index, which is 0.78 for Cas A. For thermal bremsstrahlung the photon index is:

$$\Gamma = 1 + \frac{E}{kT_{\rm e}}, \quad (3)$$

with $kT_{\rm e}$ the electron temperature. So we see that the overall value of $\Gamma = 3$ at 6.6 keV (cf. Holt et al. 1994) implies $E_c = 1.1$ keV or $kT_{\rm e} = 3.3$ keV (in agreement with Vink et al. 1996). The thermal spectrum steepens much faster than the synchrotron spectrum: at 9.0 keV the synchrotron model predicts $\Gamma = 3.2$, whereas the bremsstrahlung model predicts $\Gamma = 3.8$. So we see that some spectra fall off too rapidly to be dominated by synchrotron emission, except the spectra of the Western and Southern region.

It has been argued (Keohane et al. 1996) that in the Western region the blast wave is interacting with the molecular cloud seen in absorption towards Cas A (Bieging & Crutcher 1986). Such an event could lead to an enhanced cosmic ray production, but this hypothesis implies that the thermal emission should peak in the Western region as well since there should also be more shock heated material. The line images, which trace the thermal component, do not support this. Because the infrared image of Cas A (Lagage et al. 1996) does not peak in the Western region, depletion in dust cannot explain the relative lack of emission. In addition, sulphur and argon are not depleted in dust. However, the lack of line emission can be reconciled with an interaction between a molecular cloud and Cas A, if the electron temperature is too low to produce appreciable S, Ar and Fe K line emission in this region. The electron temperature is potentially low if the shock wave decelerates rapidly when entering the dense cloud. The weak line emission originating from the Western region may in that case come from the far side of Cas A, where the blast wave is possibly undisturbed.

Turning the attention now to the line images, we note several interesting features. First of all, little line emission originates from the Southern region. Although the VLA image also shows some lack of emission in that region, the near absence of line emission is rather puzzling. Another feature is that the morphology of the line images indicates that the remnant can be divided into roughly two halves, with the intersection running from Northeast to Southwest. Interestingly, this is also the division made on the basis of X-ray Doppler shift maps (Markert et al. 1983, Holt et al. 1994 and Tsunemi et al. 1996). Tsunemi et al. (1996) report that the Fe K line has larger Doppler shifts than the other elements, although there are some uncertainties, due the fact that non-equilibrium ionization effects may mimic Doppler shifts. If Doppler shifts are indeed larger for the Fe K lines, then this may be connected to the observation presented here that the Fe K emission in the Southeast peaks further out from the center than the emission from other elements. In this case most Fe K emission in the Southeast presumably originates from the swept up circumstellar medium, which has a larger velocity than the supernova ejecta heated by the reverse shock.

4. Conclusion

We have presented narrow band images of Cas A deconvolved with the Lucy-Richardson method. There is a clear distinction between the morphology of the continuum emission and the

line emission. The images dominated by line emission resemble each other, but we found that the iron K-shell emission in the Southeast peaks $\sim 20''$ further out from the center than the emission from other elements.

The continuum emission increasingly enhances in the Western region when going to harder X-rays, making it likely that the hard X-ray tail is coming predominantly from the Western side of the remnant. Furthermore, the difference in morphology between the line and continuum images indicates that part of the continuum emission of especially the Western region is probably synchrotron radiation.

The enhanced non-thermal emission from the Western region may be indicative of a collision of Cas A with a molecular cloud. This hypothesis does not seem to be supported by the line emission images, which should also show brightness enhancement in the West. However, a low electron temperature of the shocked molecular cloud material may circumvent this.

Our analysis provides the first images of Cas A at energies above 7 keV, which allows for the separation of the non-thermal and the thermal X-ray emission at angular scales of the order of $1'$. In the near future XMM, with its high throughput above 8 keV, will allow extension of this type of research to the arcsecond scale. The excellent photon statistics expected from this X-ray observatory will allow accurate Doppler shift measurements and will potentially reveal new details, which may provide an explanation to some of the peculiarities of the X-ray emission from the Western region.

Acknowledgements. We thank Silvano Molendi for providing us with the parameterization of the MECS PSF. M.C. Maccarone and T. Mineo acknowledge useful discussions with Bruno Sacco. Jacco Vink acknowledges pleasant and useful discussions with Glenn Allen. We thank the referee J. Dickel for some suggestions which helped to improve this article. This research has made use of data obtained through the High Energy Astrophysics Science Archive Research Center Online Service, provided by the NASA/Goddard Space Flight Center and by the NCSA Astronomical Digital Image Library (ADIL). This work was financially supported by NWO, the Netherlands Organization for Scientific Research.

References

Allen G.E., Keohane J.W., Petre R., et al., 1997, ApJ 487, L97
Anderson M.C., Rudnick L., 1995, ApJ 441, 307
Ashworth W.B., 1980, J. Hist. Astr., 11, 1
Asvarov A.I., Dogiel V.A., Guseinov O.H., Kasumov F.K., 1990, A&A 229, 196.
Bieging J.H., Crutcher R.M., 1986, ApJ 310, 853
Boella G., Butler R.C., Perola G.C., et al., 1997a, A&AS 122, 299
Boella G., Chiappetti L., Conti G., et al., 1997b, A&AS 122, 327
Favata F., Vink J., Dal Fiume D., et al., 1997, A&A 324, L49
Fesen R.A., Becker R.H., Blair W.P., 1987, ApJ 313, 378
García-Segura G., Langer N., Mac Low M.-M., 1996, A&A 316, 133
Holt S.S., Gotthelf E.V., Tsunemi H., Negoro H., 1994, PASJ 46, L15
Keohane J.W., Rudnick L., Anderson M.C., 1996, ApJ 466, 309
Keohane J.W., Gotthelf E.V., Petre R., 1998, ApJ 503, L175
Koralesky B., Rudnick L., Gotthelf E.V., Keohane J.W., 1998, ApJ 505, L27
Koyama K., Petre R., Gotthelf E., et al., 1995, Nat 378, 255
Lagage P.O., Claret A., Ballet J., et al., 1996, A&A 315, L273
Laming J.M., 1998, ApJ 499, 309
Lucy L., 1974, AJ 79, 745
Maccarone M.C., Grandi P., Mineo T., et al., 1998, In: Scarsi L., Bradt H., Giommi P., Fiore F. (eds.) The Active X-ray Sky. Nuclear Physics B Proc. Suppl. 69, Elsevier Science, 1998
Markert T.H., Canizares C.R., Clark G.W., Winkler P.F., 1983, ApJ 268, 13
Reed J.E., Hester J.J., Fabian A.C., Winkler P.F., 1995, ApJ 440, 706
Reynolds S.P., 1997, ApJ 493, 375
Reynolds S.P., Chevalier R.A., 1981, ApJ 245, 912
Richardson W.H., 1972, J. Opt. Soc. Am. 62, 55
Tanimori T., Hayami Y., Kamie S., et al., 1998, ApJ 497, L25
The L.-S., Leising M.D., Kurfess J.D., et al., 1996, A&AS 120, 357
Tsunemi H., Kinugasa K., Ohno Y., 1996, MPE report 263, In: Trümper J. (ed.) Röntgenstrahlung in the Universe
Van den Bergh S., Kamper K.W., 1983, ApJ 268, 129
Vink J., Kaastra J.S., Bleeker J.A.M., 1996, A&A 307, L41
Vink J., Bloemen H., Kaastra J.S., Bleeker J.A.M., 1998, A&A 339, 201